CHAPTER FOUR

Optical Imaging of Cell Death in Traumatic Brain Injury Using a Heat Shock Protein-90 Alkylator

Based on

Xie BW*, Park D*, Van Beek ER, Blankevoort V, Orabi Y, Que I, Kaijzel EL, Chan A, Hogg PJ, Löwik CW. ***Cell Death Dis.*** 2013; 4: e473.

Abstract

Traumatic brain injury is a major public health concern and is characterized by both apoptotic and necrotic cell death in the lesion. Anatomical imaging is usually employed to assess traumatic brain injuries and there is a need for imaging modalities that provide complementary cellular information. We sought to non-invasively image cell death in a mouse model of traumatic brain injury using a near-infrared fluorescent conjugate of a synthetic heat shock protein-90 alkylator, 4-(N-(S-glutathionylacetyl) amino) phenylarsonous acid (GSAO). GSAO labels both apoptotic and necrotic cells coincident with loss of plasma membrane integrity. The optical GSAO specifically labelled apoptotic and necrotic cells in culture and did not accumulate in healthy organs or tissues in the living mouse body. The conjugate is a very effective imager of cell death in brain lesions. The optical GSAO was detected by fluorescence intensity and GSAO bound to dying/dead cells was detected from prolongation of the fluorescence lifetime. An optimal signal-to-background ratio was achieved as early as three hours after injection of the probe and the signal intensity positively correlated with both lesion size and probe concentration. This optical GSAO offers a convenient and robust means to non-invasively image apoptotic and necrotic cell death in brain and other lesions.

Keywords

Traumatic brain injury, cryolesion, apoptosis, necrosis, GSAO, optical imaging

Abbreviations

DMP, dimercaptopropanol; GSAO, 4-(N-(S-glutathionylacetyl) amino) phenylarsonous acid; GSCA, 4-(N-((S-glutathionyl)acetyl)amino)benzoic acid; AF750, Alex Flour 750; Hsp90, heat shock protein 90; PI, propidium iodide; ROI, region of interest; TUNEL, TdT-mediated dUTP nick-end labelling

Introduction

Traumatic brain injury is estimated to affect 2% of the US population and cost about $60 billion annually [1,2]. The nature of the injuries depends on the type, severity and location of the insult but are usually characterized by primary mechanical damage and hemorrhage followed by secondary damage due to disruption of the blood-brain-barrier and associated inflammation [3]. The secondary insult occurs hours to days after the primary insult and is amenable to therapeutic intervention. Computer tomography and magnetic resonance imaging are used to assess morphological changes in traumatic brain injury that occur in the later stages of the injury [4]. Treatment of the secondary damage would be facilitated by imaging modalities that report on changes in the lesion at the cellular level. Traumatic brain injury is characterized by both apoptotic and necrotic cell death in the lesion [3] and this is what we sought to image in this study.

An established model of traumatic brain injury in mice is the cryolesion. A sharp delineated area of neuronal cell death is induced in the mouse brain by applying a liquid nitrogen cooled rod to the skull [5]. Cell death within brain cryolesions occurs via two distinct mechanisms. Firstly, intracellular ice crystals rupture the cell membrane causing direct cell damage[6]. Secondly, injury to endothelial cell junctions results in increased vascular permeability, oedema, thrombosis, and ultimately failure of the microcirculation, leading to a secondary ischemic assault[7]. Whilst the centre of the lesion is characterized by tissue necrosis, apoptosis is also observed in the periphery as early as 12 hours post injury [5]. The latter is thought to occur via mitochondrial permeabilization following increased expression of Bax [8]. Upregulation of genes involved in neuronal survival or regeneration is also observed [9,10]. This lesion bears many features of neurotrauma [6,7]. Here we have non-invasively imaged the cell death in these lesions using a heat shock protein 90 (Hsp90) alkylator [11].

GSAO (4-(N-(S-glutathionylacetyl) amino)phenylarsonous acid) is a tripeptide trivalent arsenical that rapidly accumulates in the cytoplasm of dying cells in culture and in murine tumors [11]. It is retained in the cell predominantly through covalent reaction with the Cys597 and Cys598 residues of Hsp90, which is the most abundant protein chaperone in mammalian cells [12]. The As(III) atom of GSAO cross-links the Hsp90 Cys597 and Cys598 sulfur atoms forming a stable cyclic dithioarsinite [13,14]. This complex is effectively irreversible in biological milieu. There are very few appropriately spaced cysteine thiols in the extracellular environment so GSAO is largely unreactive until it crosses the plasma membrane. GSAO does not cross the intact plasma membrane of viable or early-stage apoptotic cells but enters mid- to late-stage apoptotic cells when the plasma membrane is compromised.

In this study we have investigated the utility of a near-infrared fluorescent conjugate of GSAO to non-invasively detect cell death in mouse brain cryolesions [15-19]. GSAO was conjugated to the near-infrared fluorophore, Alex Flour 750 (GSAO-

AF750), to maximize tissue penetration of the fluorescent signal and to minimize the complications of tissue auto-fluorescence [20].

Results

GSAO-AF750 specifically labels apoptotic and necrotic cells in culture

Conjugation of AF750 to the primary amine of the λ-glutamyl residue of GSAO did not affect its capacity to specifically label dying cells. The specificity and sensitivity of labelling of dying/dead cells by AF750-tagged GSAO was examined in *in vitro* models of apoptotic (human Jurkat T cells treated with staurosporine) and necrotic (4T1-luc2 mouse breast cancer cells treated with dry ice) cell death. Staurosporine is a microbial alkaloid and broad spectrum protein kinase inhibitor that triggers mitochondrial-mediated apoptotic cell death, while snap freezing of cells ruptures the plasma membrane resulting in necrotic cell death. The probe was detected from the fluorescence intensity of the AF750 tag.

Apoptotic Jurkat T cells were labelled with the late stage apoptosis/necrosis marker, propidium iodide (PI), and either GSAO-AF750 or the phosphatidylserine ligand, PSVue®794[18]. GSAO-AF750 and PSVue®794 labelled dying and dead PI-positive cells in staurosporine treated samples (Fig. 1a). There were subpopulations of cells that labelled with PSVue®794 but not PI (Fig. 1a, top panels) and labelled with PI but not GSAO-AF750 (Fig. 1a, middle panels). PSVue®794, like annexinV, binds exteriorized phosphatidylserine on cell membranes of early- and late-stage apoptotic cells[21], so the PSVue®794-positive, PI-negative population likely represents early stage apoptotic cells. The PI-positive cells that did not label with GSAO-AF750 possibly represents cell fragments that are devoid of the GSAO-AF750 ligand, Hsp-90.

The selectivity of GSAO-AF750 for dying and dead cells is mediated by the trivalent arsenic moiety. This was confirmed using two different controls. The synthetic dithiol, dimercaptopropanol (DMP), sequesters the trivalent arsenic moiety of GSAO, while GSCA-AF750 contains a chemically inert carboxylic acid group in place of the reactive trivalent arsenic moiety. Pre-treatment with DMP effectively ablated labelling of dying/dead cells by GSAO-AF750, but not by PSVue®794 (Fig. 1a, right panels). The mean GSAO-AF750 fluorescence intensity of PI-positive cells was ~60-fold less when cells were pre-treated with DMP. In addition, GSCA-AF750 did not label dying/dead PI-positive cells in staurosporine treated samples. The mean GSCA-AF750 fluorescence intensity of PI-positive cells was > 250-fold less than cells stained with GSAO-AF750 (Fig. 1a, bottom panels). Viable untreated cells did not stain with any of the compounds. These findings are consistent with our initial characterization of the compound [11] and are in accordance with its reaction with Hsp-90.

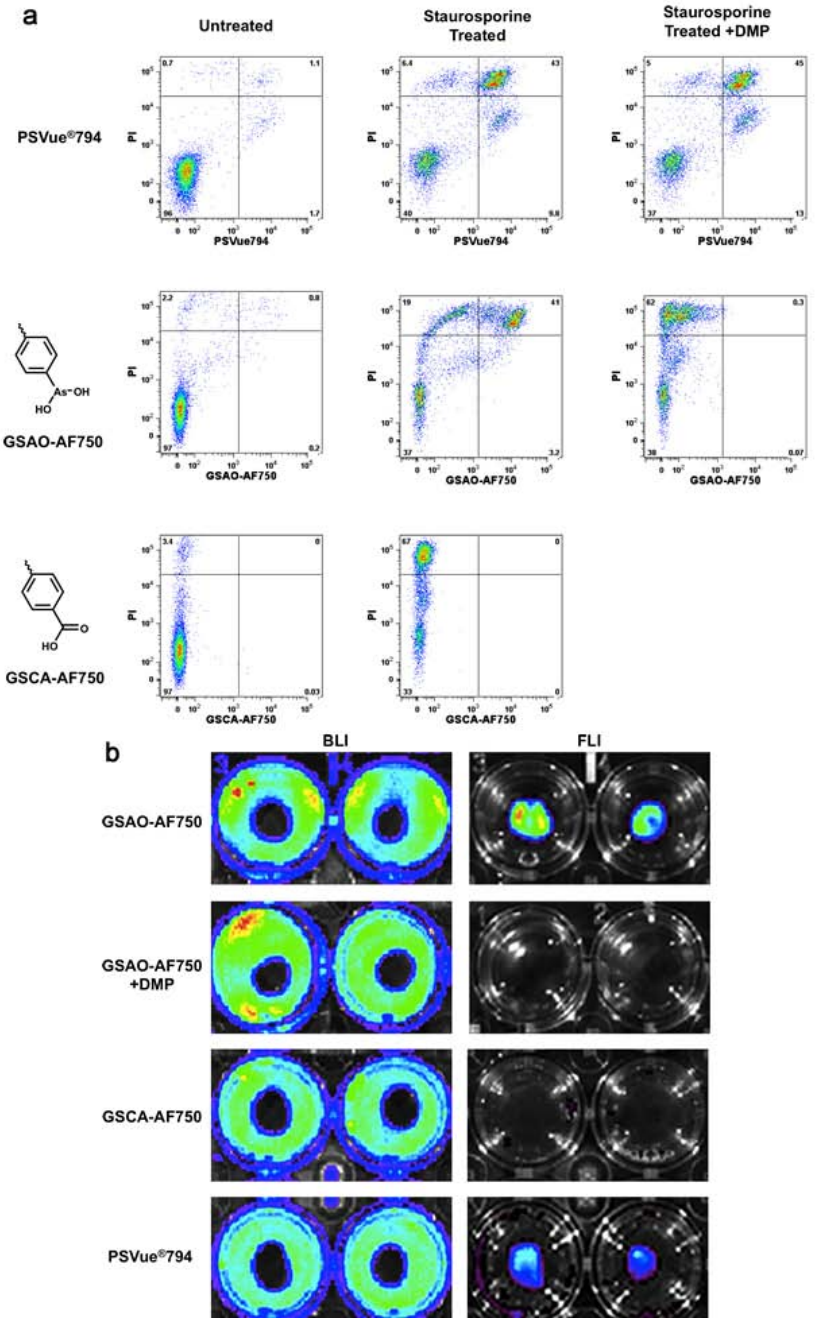

Figure 1. GSAO-AF750 specifically labels apoptotic and necrotic cells in culture. (a) Apoptotic death in Jurkat A3 T cells was triggered with staurosporine for 24 h and the cells subsequently incubated with PI (all panels) and either with PSVue®794 (upper panels), GSAO-AF750 (middle panels), or control GSCA-AF750 (lower panels) and labelling analysed by flow cytometry. In some samples (right panels), cells were pre-incubated with the trivalent arsenic ligand, DMP, prior to GSAO-AF750 or PSVue®794 staining. The numbers depicted in the scatter

plots represent the percentage of cells in the quadrants. (b) Necrotic death in confluent monolayers of 4T1-luc2 mouse breast cancer cells was induced by applying dry ice to the underside of the culture well and the cells subsequently incubated either with GSAO-AF750, GSCA-AF750 or PSVue®794. In some wells, cells were pre-treated with DMP prior to incubation with GSAO-AF750. Cells were imaged for fluorescence (right panels) and then for bioluminescence following by incubation with D-luciferin (left panels).

Necrotic 4T1 mouse breast cancer cells expressing the l*uc2* luciferase reporter gene were incubated with either GSAO-AF750, GSCA-AF750 or PSVue®794. Necrotic cell death was induced by applying dry ice to the underside of the culture well, resulting in a discrete central region of dead cells surrounded by an external ring of healthy cells. The external ring of viable cells was imaged by bioluminescence following incubation with D-luciferin (Fig. 1b, indicated by blue/green). Necrotic cells are deficient in ATP, which is a substrate for the luciferin/luciferase reaction, so they do not emit light. Fluorescence imaging revealed that both GSAO-AF750 and PSVue®794, but not control GSCA-AF750, selectively labelled the area of dead cells in the centre of the well (Fig. 1b). Any probe did not stain the ring of healthy cells. Pre-treatment of the cultures with DMP totally abolished staining by GSAO-AF750.

In vivo and *ex vivo* imaging of brain lesion cell death in mice with GSAO-AF750

The suitability of GSAO-AF750 for non-invasive imaging of apoptotic and necrotic cell death in the living animal was examined in a murine model of traumatic brain injury. A focal area of cell death is induced in the mouse brain by applying a liquid nitrogen insult to the skull[5]. The cryolesion is characterized by both apoptotic and necrotic cell death and shares many features with neurotrauma [6,7].

A 60 sec brain cryolesion was induced in the front part of the right parietal lobe, followed by tail vein injection of GSAO-AF750 or GSCA-AF750 (1 mg/kg). Whole body fluorescence imaging was performed at 1, 3, 6 and 24 h after probe injection. GSAO-AF750 and GSCA-AF750 were, with the exception of the kidneys, eliminated from the body within 3 h of administration (Fig. 2a). Both compounds were observed to be excreted in the urine, in accordance with the kidney localization at earlier time points. A strong GSAO-AF750 signal, but not for control GSCA-AF750, was observed at all times points at the brain lesion site (Fig. 2a). In one mouse, a 3D sectional view was formed to depict the relative concentration of GSAO-AF750 in the brain lesion (Fig. 3). The GSAO-AF750 signal in brain lesions remained steady between 1 and 6 h after probe injection and dropped by 24 h (Fig. 2b). The control GSCA-AF750 signals were 50-100 fold lower than those obtained with GSAO-AF750 at all time points ($p < 0.001$). The signal to background ratio for GSAO-AF750 (lesion versus adjacent healthy hemisphere) was approximately 3:1 at all time points.

The brains of the mice were excised for *ex vivo* imaging 24 h after probe injection. Accumulation of GSAO-AF750 in the lesion site was clearly evident (Fig. 2c). Some GSCA-AF750 was also detected in the lesion site, however the signal intensity was ~7-fold lower than that for GSAO-AF750 ($p < 0.001$) (Fig. 2d).

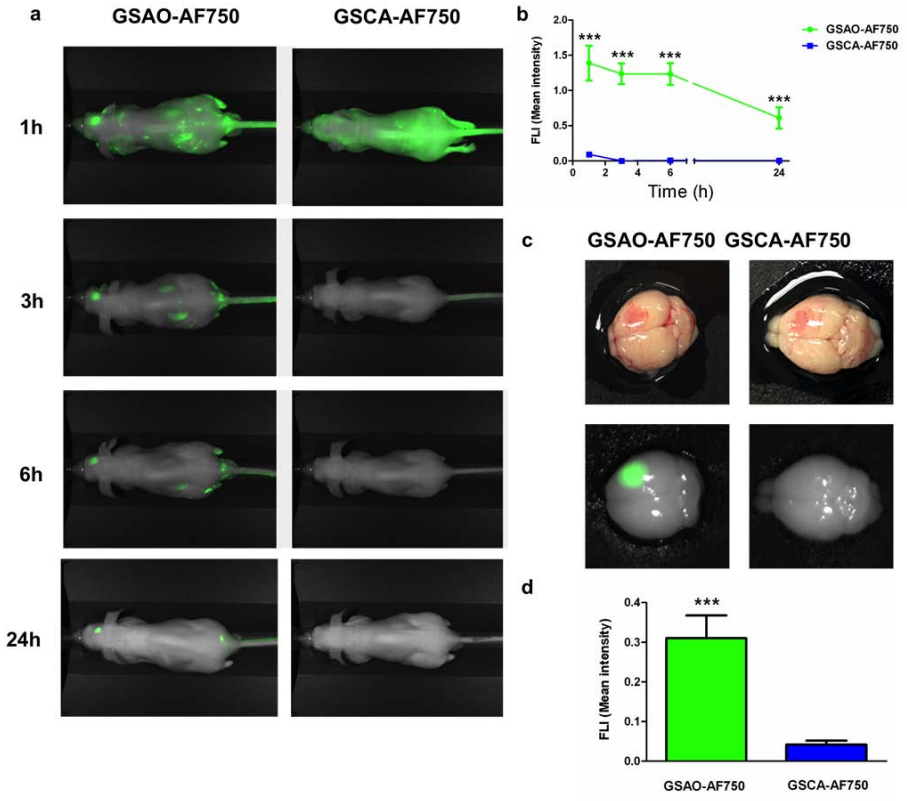

Figure 2. In vivo and ex vivo imaging of brain lesion cell death in mice with GSAO-AF750. (a) A 60 sec brain cryolesion was induced in the front part of the right parietal lobe, followed by tail vein injection of 1 mg/kg GSAO-AF750 (left panels) or GSCA-AF750 (right panels) and whole body fluorescence imaging was performed at 1, 3, 6 and 24 h after probe injection. (b) Quantification of the integrated mean intensity of GSAO-AF750 and GSCA-AF750 signals in the brain lesion over time. GSAO-AF750 versus GSCA-AF750 intensities were calculated at 1, 3, 6 and 24 h (***, $p < 0.001$). (c) The brains of the mice were excised for *ex vivo* imaging 24 h after probe injection. Bright field images of a representative GSAO-AF750 and control GSCA-AF750 brain, showing a red discolouration of the lesion site, are shown in the top panel, while the fluorescence images of the same brains are shown in the bottom panel. (d) Quantification of the *ex vivo* integrated mean intensity of the AF750 signal. GSAO-AF750 versus GSCA-AF750 fluorescence intensity was calculated (***, $p < 0.001$).

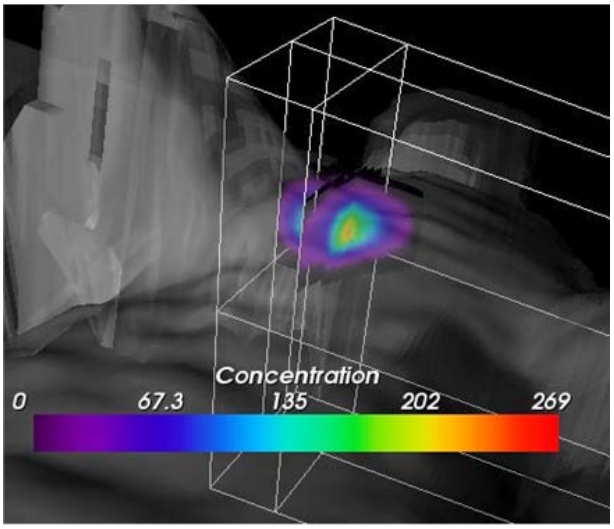

Figure 3. 3D sectional view depicting the relative concentration of GSAO-AF750 in a brain cryolesion. A concentration gradient of GSAO-AF750 radiates from the centre of the lesion.

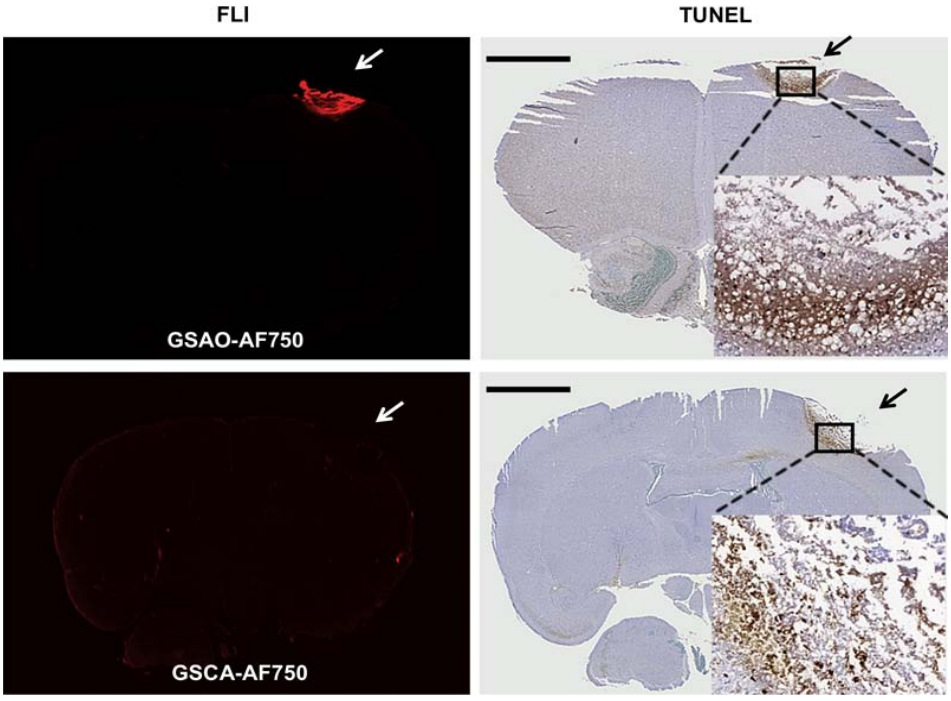

Figure 4. GSAO-AF750 labels dying/dead brain lesion cells in mice. The brains of mice subjected to a cryolesion were excised and sectioned 24 h after GSAO-AF750 or control GSCA-AF750 injection. The sections were examined for AF750 fluorescence (left panels) and cell death using TUNEL staining (right panels). GSAO-AF750, but not control GSCA-AF750, was observed in the lesion and co-localised with TUNEL-positive areas.

The specificity of GSAO-AF750 for dying and dead brain cells was confirmed *ex vivo* by analysis of brain sections. Fluorescence imaging and immunohistochemistry revealed co-localisation of GSAO-AF750 with TUNEL-positive cells in the cryolesion (Fig. 4).

In vivo and *ex vivo* imaging of brain lesion cell death with GSAO-AF750 is a function of lesion size and probe concentration

The influence of brain lesion size and the dose of GSAO-AF750 on the signal intensity was evaluated. Mice bearing a 60 sec cryolesion were administered 0.1 or 1 mg/kg GSAO-AF750, and mice bearing a 5 sec cryolesion were administered 1 mg/kg GSAO-AF750 (Fig. 5a). All mice were imaged at 1, 3 and 6 h following probe injection. At all time points, total fluorescence intensity in the lesions of mice injected with 0.1 mg/kg GSAO-AF750 was 30- to 50-fold less than in those injected with 1 mg/kg GSAO-AF750 ($p < 0.01$ at 1 and 6 h and $p < 0.05$ at 3 h). In addition, the total fluorescence intensity of lesions in mice injected with 1 mg/kg GSAO-AF750 was ~5-fold lower in mice with a 5 sec cryolesion compared to those with a 60 sec cryolesion ($p < 0.05$ at all time points). These findings were confirmed *ex vivo* by measuring the fluorescence intensity of the excised brains 6 h after GSAO-AF750 injection (Fig. 5b).

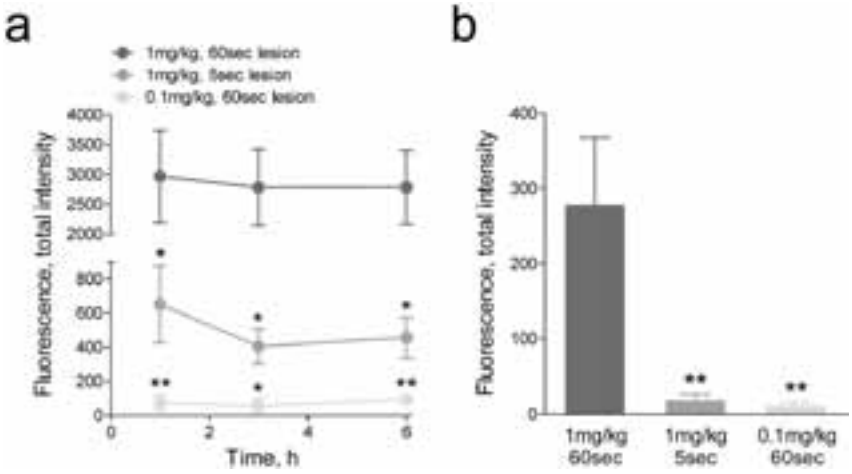

Figure 5. In vivo and ex vivo imaging of brain lesion cell death with GSAO-AF750 is a function of lesion size and probe concentration. (a) *In vivo* quantification of GSAO-AF750 signal intensity in the cryolesion over time. GSAO-AF750 fluorescence intensity was compared between mice bearing 5 s and 60 s cryolesions (**, $p < 0.01$; *, $p < 0.05$), or injected with a lower concentration of GSAO-AF750 (*, $p < 0.05$ at 1, 3 and 6 h). (b) The brains of the mice were excised for *ex vivo* imaging 6 h after probe injection and the integrated mean intensity of the AF750 signal was measured. GSAO-AF750 fluorescence intensity was significantly lower in brains bearing a 5 s cryolesion or injected with 0.1 mg/kg GSAO-AF750 (**, $p < 0.01$).

Fluorescence lifetime imaging of GSAO-AF750 bound to dying/dead cells in culture and in brain lesions

The fluorescence lifetime of unbound GSAO-AF750 versus bound to dying/dead cells was measured in necrotic breast cancer cells and in brain cryolesions. The lifetime of free GSAO-AF750 and control GSCA-AF750 in phosphate buffered saline was 0.58-0.61 ns, while the weighted average single fluorescence lifetime of GSAO-AF750 lengthened to 0.89 ns when bound to necrotic breast cancer cells (Fig. 6a). Negative controls were no binding of GSAO-AF650 in the presence of DMP and no binding of GSCA-AF750 (Fig. 6a). A single exponential fit of the time point spread function curve produced a weighted average fluorescence lifetime of 0.97-1.05 ns for GSAO-AF750 in brain cryolesions (Fig. 6b), which is comparable to the lifetime measured in cultured dying/dead cells.

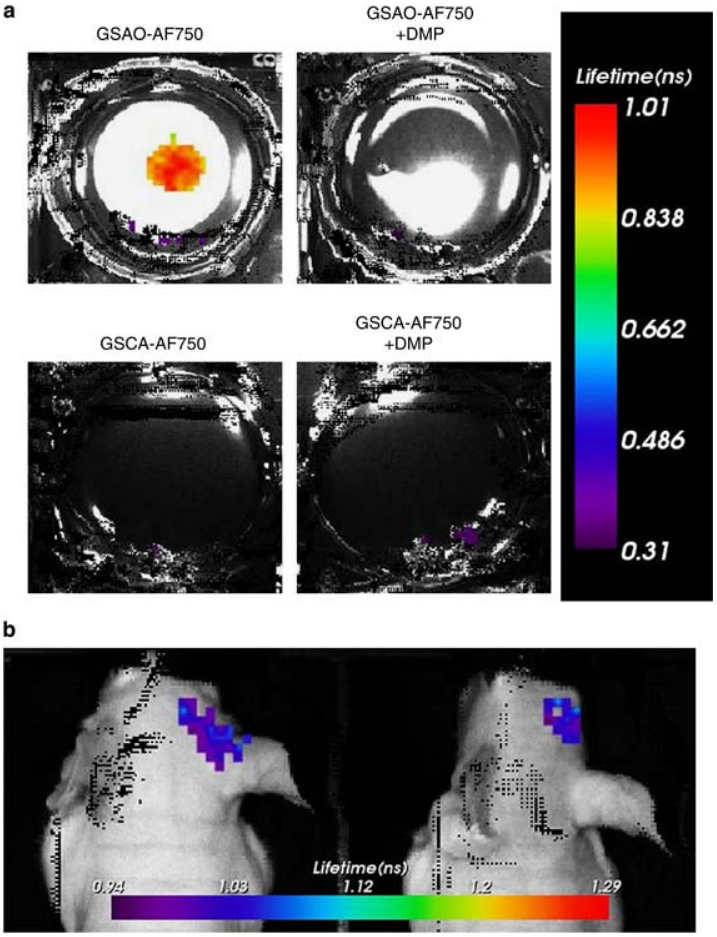

Figure 6. Fluorescence lifetime imaging of GSAO-AF750 bound to dying/dead cells. (a) Single exponential

fluorescence lifetime analysis of GSAO-AF750 labelling of dying/dead cells in culture. Focal cell death in confluent monolayers of 4T1-luc2 mouse breast cancer cells was induced by applying dry ice to the underside of the culture well and the cells subsequently incubated with GSAO-AF750 (top left well), GSAO-AF750 with DMP (top right well), GSCA-AF750 (bottom left well) or GSCA-AF750 with DMP (bottom right well). (b) Single exponential fluorescence lifetime analysis of GSAO-AF750 labelling of dying/dead cells in brain cryolesions of two different mice.

Discussion

The effectiveness of a non-invasive imaging agent is mostly a product of the selectivity for its biological target and the volume of its distribution. Imaging sensitivity and resolution is enhanced when the reporter agent accumulates in high concentration in a small volume. We employed herein a small molecule that targets Hsp90 of apoptotic and/or necrotic cells.

Hsp90 is, in principle, an attractive imaging target as it is one of the most abundant proteins in the mammalian cell cytoplasm. Alkylation of Hsp90 by GSAO in dying/dead cells results in high concentration of the compound in the largest compartment of the cell [11]. This is in contrast to the ligands that target phosphatidylserine exposed on the exterior of the plasma membrane during apoptosis [22-24], for instance, which are restricted to the cell surface compartment. Conjugation of the near-infrared fluorophore, AF750, to the λ-glutamyl amine of GSAO did not affect its specific labelling of apoptotic and necrotic cells in culture. In accordance with previous studies [11], the labelling was a function of the dithiol alkylating chemistry of the As(III) moiety of GSAO-AF750.

Importantly, as shown herein, GSAO-AF750 has very favorable pharmacokinetics and biodistribution in mice. It is secreted via the renal circulation and does not accumulate in healthy organs or tissues. Three hours after intravenous administration it is found only in the kidneys. Less than optimal pharmacokinetics and biodistribution has limited the development of a number of cell death imaging agents to date. This has been the case for the protein ligands that recognize phosphatidylserine [25,26], although a new generation of small molecule phosphatidylserine ligands may overcome these issues [18,27].

GSAO-AF750 specifically labels dying and dead cells in brain cryolesions. The AF750 signal was apparent as early as one hour in the lesions and remained unchanged for approximately six hours. The signal to background ratio was ~3:1 at all time points and signal intensity was a function of both lesion size and probe concentration. The specificity of GSAO-AF750 for dying and dead brain cells was confirmed *ex vivo*. Notably, cells in the periphery of the brain lesion stained strongly by TUNEL, while cells in the centre stained weakly. This is indicative of the apoptotic and necrotic cells, respectively, in the lesion [5]. Both cell types in the lesion stained with GSAO-AF750, which is in accordance with the cell culture results showing that GSAO-AF750 labels both apoptotic and necrotic cells.

An advantage that optical agents can have over other reporter groups is a change in the fluorescence properties of the fluorophore when it is bound to its

target [28-33]. Alteration of the microenvironment of the fluorescent moiety upon target binding can result in a shortening or lengthening of the fluorescence lifetime. This difference can be used to distinguish between unbound and bound agent in the target tissue as it is independent of intensity variations or local concentrations of the fluorophore. The fluorescence lifetime of GSAO-AF750 increased from 0.58-0.61 to 0.89 ns when bound to necrotic breast cancer cells and to 0.97-1.05 ns when bound in brain cryolesions. The significantly longer fluorescence lifetime when bound to its target will be a useful parameter when optimizing the signal-to-background contrast in future studies that explore other experimental and clinical applications of GSAO-AF750.

Optical imaging technologies, including fuorescence-guided surgery and endoscopy, intravascular fluorescence imaging and photoacoustic applications in cardiovascular disease, dermatology and cancer, have advanced rapidly in recent years [34,35]. In the last decade, optical imaging has moved from gross assessment of structure and morphology to imaging of biological processes that underlie disease. Although, the development of the hardware to measure light in the human body has outpaced the development of specific probes that report on cellular events. GSAO-AF750 shows promise for the pre-clinical and clinical imaging of cell death in brain and other lesions.

Acknowledgments

This study is supported by the Dutch Center for Translational Molecular Medicine, project MUSIS (grant 03O-202), the ENCITE project 201842, the National Health and Medical Research Council of Australia and the Cancer Council New South Wales.

Materials and Methods

Ethical statement

All animal experiments were approved for animal health, ethics, and research by the Animal Welfare Committee of Leiden University Medical Center, the Netherlands (Approval DEC number 11198). All the mice were purchased from Charles River Laboratories, France and received humane care and maintenance in compliance with the “Code of Practice Use of Laboratory Animals in Cancer Research” (Inspectie W&V, July 1999).

Synthesis of near-infrared GSAO and GSCA conjugates

A solution of AF750 (λ_{ex}:752nm, λ_{em}:776nm) succinimidyl ester (10 mg/mL in DMSO, Invitrogen) was added to GSAO (4.2 mg/mL) or control 4-(N-((S-glutathionyl)acetyl)amino)benzoic acid (GSCA, 5.9 mg/mL), in 0.1 M bicarbonate buffer, pH 8.3 and incubated for 60 min in the dark in the presence of nitrogen. The molar ratio of fluorophore to pendant was ~1:1. Unreacted fluorophore was quenched by adding 10 mM glycine. The conjugate was separated from unreacted fluorophore by passing the reaction through at least two Sephadex G10 spin columns equilibrated with 0.1 M bicarbonate buffer, pH 8.3 (Sigma). The unreacted dye binds to the Sephadex matrix while the conjugate elutes in the void volume. Purity of the conjugates was confirmed by HPLC (1200 Series; Agilent Technologies) on a Zorbax Eclipse XDB-C18 column (4.6 x 150 mm, 5 µm; Agilent Technologies) using a mobile phase of acetonitrile-water (25:75 vol/vol), flow rate of 0.5 mL per min and detection by absorbance at 256 nm. The conjugates were resolved from unreacted GSAO or GSCA by this method. Purity was also assessed by thin layer chromatography using a 3:1:1 butanol/acetic acid/water mobile phase. The purity of GSAO-AF750 and GSCA-AF750 was >95%.

Cell culture

Jurkat A3 cells (ATCC) and mouse breast cancer cells 4T1-luc2 expressing the codon-optimized luciferase gene *luc2* (Caliper Life Sciences) were cultured in RPMI-1640 medium supplemented with 10% fetal bovine serum and 1 U/mL penicillin/streptomycin. All other cell culture reagents were from Gibco.

In vitro validation of GSAO-AF750 and GSCA-AF750 via flow cytometry

Jurkat A3 cells were seeded at a density of 5 x 10^5 cells per mL and incubated with or without 4 µM staurosporine (Sigma) for 24 h. Cells were washed twice with ice cold phosphate-buffered saline and incubated at room temperature with 1 µM GSAO-AF750 or control GSCA-AF750 for 15 min with shaking. Alternatively, cells were washed in phenol red free RPMI-1640 medium and stained with PSVue®794 (Polysciences, Inc), as per the manufacturer's instructions. On some occasions the cells were pre-treated with DMP (50 µM, Sigma), for 1 min. Cells were washed again and incubated with PI (1 µg/mL, Invitrogen) for 15 min in the dark. Flow cytometry was performed using a BD™ LSR II Flow Cytometer with a

high power 200mW, 628 nm red excitation laser, a 40mW, 786nm near-infrared excitation laser and a 100mW, 488nm excitation laser (BD Biosciences). Data were analyzed using FlowJo software version 8.7.

In vitro cryo-induced cell death assay

4T1-luc2 cells were seeded onto 12-well plates and grown to confluency in complete RPMI-1640 medium. The medium was discarded and a bar of dry ice 3-5 mm in diameter applied to the underside of the culture well for 15 sec. GSAO-AF750, GSCA-AF750, or PSVue®794 (0.4 µM in 500 µL medium) was added to the cells and incubated for 15 min at 37 °C. The cells were gently washed twice with phosphate-buffered saline and imaged using the IVIS Spectrum (Caliper Life Sciences) (excitation 710 nm, emission 780 nm). Subsequently, D-luciferin (150 mg/kg in 5 µL PBS) (SynChem, Inc) was added to each well for 10 min and bioluminescence images acquired using the same machine. To complement the intensity measurements, fluorescence lifetime images of 4T1-luc2 cells on 12-well plates in the presence of GSAO-AF750 or control GSCA-AF750 were determined using a time domain optical imager (Optix MX3). Tubes of GSAO-AF750 and GSCA-AF750 in their free state were also scanned in order to establish a fluorescence lifetime reference for the subsequent *in vivo* studies.

In vivo murine model of cryo-induced traumatic brain injury

A brain cryolesion was applied as described previously with minor modifications [18]. In short, six-week old male BALB/c nu/nu mice (Charles River Laboratories, France) were sedated with 2-3% isoflurane and a cryolesion induced in the parietal lobe of the right cerebral hemisphere. A metal rod of 3 mm in diameter was pre-cooled with liquid nitrogen and applied to the skull for 5 or 60 sec. Mice were allowed to recover from the anaesthetic and observed for any adverse symptoms resulting from the cryolesion. Mice were then injected intravenously with either GSAO-AF750 or control GSCA-AF750 (0.1 mg/kg or 1 mg/kg in 100 µL PBS) and imaged with the Pearl® Impulse Small Animal Imaging System (LI-COR Biosciences) at 1, 3, 6 and 24 h. Prior to imaging mice were wiped with 70% v/v ethanol to remove any of the compounds excreted in the urine and contaminating the skin. At the experiment endpoint the mice were sacrificed by cervical dislocation and the brains excised for *ex vivo* fluorescence imaging. Images were acquired at 800 nm at a resolution of 85 µm.

The fluorescent signal was digitized and electronically displayed as a pseudocolor overlay on a gray scale white light image of the animal. The data was analyzed using Pearl® Impulse Software, Version 2.0. Total AF750 fluorescence intensity was determined by drawing a region of interest (ROI) over the area in

which the cryolesion was induced. The size and shape of the ROI was the same for each time point. An ROI of equivalent size was then drawn over the adjacent hemisphere to determine the background signal and this was subtracted from the lesion signal. Where integrated mean fluorescence intensity of AF750 is shown, the value has been corrected for the area of the ROI. Results are depicted as mean ± standard error of the mean. Statistical analysis was performed using a Student's t-test.

Whole mouse fluorescence imaging was performed using the Optix MX3. Animals were placed on a heated five-mouse bed imaging platform so that mice administered GSAO-AF750 and control GSCA-AF750 could be compared side-by-side. A 735 nm, 80 MHz pulse diode laser was used for excitation and raster-scanning, performed in 1 mm steps. Photon emission was captured by time-correlated single photon counting with a 755 nm long pass filter and data were recorded as temporal point spread functions. Image analysis and fluorescence lifetime calculations were performed using Optiview 3.0 software (ART). Rectangular ROIs were drawn around the head region to initially determine the single exponential fluorescence lifetime. This is the weighted average of all the fluorescence lifetime values.

Histological validation

Brains were fixed in 4% formaldehyde, embedded in paraffin and 8 µm sections were prepared and imaged using the LI-COR Odyssey Infrared Imager 9120 (LI-COR Biosciences) at 800 nm. Afterwards, the sections were subjected to TdT-mediated dUTP nick-end labelling (TUNEL) staining (Promega) to confirm accumulation of GSAO-AF750 in dying and dead cells.

References

1. Faul, M., Xu, L., Wald, M.M. & Coronado, V.G. Traumatic brain injury in the United States: emergency department visits, hospitalizations, and deaths, 2002-2006. *National Center for Injury Prevention and Control, Centers for Disease Control and Prevention*, 1-71 (2010).
2. Thurman, D.J., Alverson, C., Dunn, K.A., Guerrero, J. & Sniezek, J.E. Traumatic brain injury in the United States: A public health perspective. *The Journal of head trauma rehabilitation* **14**, 602-615 (1999).
3. Werner, C. & Engelhard, K. Pathophysiology of traumatic brain injury. *British journal of anaesthesia* **99**, 4-9 (2007).
4. Kim, J.J. & Gean, A.D. Imaging for the diagnosis and management of traumatic brain injury. *Neurotherapeutics* **8**, 39-53 (2011).
5. Steinbach, J.P., Weissenberger, J. & Aguzzi, A. Distinct phases of cryogenic tissue damage in the cerebral cortex of wild-type and c-fos deficient mice. *Neuropathol. Appl. Neurobiol.* **25**, 468-480 (1999).
6. Meryman, H.T. Mechanics of freezing in living cells and tissues. *Science* **124**, 515-521 (1956).
7. Gage, A.A., Baust, J.M. & Baust, J.G. Experimental cryosurgery investigations in vivo. *Cryobiology* **59**, 229-243 (2009).
8. Wen, J.*, et al.* Cryoablation induces necrosis and apoptosis in lung adenocarcinoma in mice. *Technol Cancer Res Treat* **6**, 635-640 (2007).
9. Margulies, S. & Hicks, R. Combination therapies for traumatic brain injury: prospective considerations. *J. Neurotrauma* **26**, 925-939 (2009).
10. Quintana, A.*, et al.* Differential role of tumor necrosis factor receptors in mouse brain inflammatory responses in cryolesion brain injury. *Journal of neuroscience research* **82**, 701-716 (2005).
11. Park, D.*, et al.* Noninvasive imaging of cell death using an Hsp90 ligand. *J Am Chem Soc* **133**, 2832-2835 (2011).
12. Nardai, G., Sass, B., Eber, J., Orosz, G. & Csermely, P. Reactive cysteines of the 90-kDa heat shock protein, Hsp90. *Arch. Biochem. Biophys.* **384**, 59-67 (2000).
13. Adams, E., Jeter, D., Cordes, A.W. & Kolis, J.W. Chemistry of Organometalloid Complexes with Potential Antidotes - Structure of an Organoarsenic(Iii) Dithiolate Ring. *Inorg Chem* **29**, 1500-1503 (1990).
14. Dilda, P.J. & Hogg, P.J. Arsenical-based cancer drugs. *Cancer treatment reviews* **33**, 542-564 (2007).
15. Grzybicki, D.*, et al.* Expression of monocyte chemoattractant protein (MCP-1) and nitric oxide synthase-2 following cerebral trauma. *Acta Neuropathol* **95**, 98-103 (1998).
16. Hotta, N.*, et al.* Expression of glia maturation factor beta after cryogenic brain injury. *Brain Res. Mol. Brain Res.* **133**, 71-77 (2005).
17. Siren, A.L.*, et al.* Global brain atrophy after unilateral parietal lesion and its prevention by erythropoietin. *Brain* **129**, 480-489 (2006).
18. Smith, B.A.*, et al.* Multicolor fluorescence imaging of traumatic brain injury in a cryolesion mouse model. *ACS Chem Neurosci* **3**, 530-537 (2012).
19. Stoffel, M.*, et al.* Identification of brain tissue necrosis by MRI: validation by histomorphometry. *J. Neurotrauma* **21**, 733-740 (2004).
20. Xie, B.W.*, et al.* Dual-wavelength imaging of tumor progression by activatable and targeting near-infrared fluorescent probes in a bioluminescent breast cancer model. *PLoS One* **7**, e31875 (2012).
21. Hanshaw, R.G. & Smith, B.D. New reagents for phosphatidylserine recognition and detection of apoptosis. *Bioorg. Med. Chem.* **13**, 5035-5042 (2005).
22. Blankenberg, F.G. In vivo imaging of apoptosis. *Cancer Biol Ther* **7**, 1525-1532 (2008).
23. Zhao, M. In vivo apoptosis imaging agents and strategies. *Anticancer Agents Med Chem* **9**, 1018-1023 (2009).
24. Niu, G. & Chen, X. Apoptosis imaging: beyond annexin V. *J. Nucl. Med.* **51**, 1659-1662 (2010).
25. Kahlem, P., Dorken, B. & Schmitt, C.A. Cellular senescence in cancer treatment: friend or foe? *The Journal of clinical investigation* **113**, 169-174 (2004).
26. Lederle, W.*, et al.* Failure of annexin-based apoptosis imaging in the assessment of antiangiogenic therapy effects. *EJNMMI Res* **1**, 26 (2011).

27. Beekman, C.A.*, et al.* Questioning the value of (99m)Tc-HYNIC-annexin V based response monitoring after docetaxel treatment in a mouse model for hereditary breast cancer. *Applied radiation and isotopes : including data, instrumentation and methods for use in agriculture, industry and medicine* **69**, 656-662 (2011).
28. Akers, W.J., Berezin, M.Y., Lee, H. & Achilefu, S. Predicting in vivo fluorescence lifetime behavior of near-infrared fluorescent contrast agents using in vitro measurements. *J Biomed Opt* **13**, 054042 (2008).
29. Ardeshirpour, Y.*, et al.* In vivo fluorescence lifetime imaging monitors binding of specific probes to cancer biomarkers. *PLoS One* **7**, e31881 (2012).
30. Erten, A.*, et al.* Enhancing magnetic resonance imaging tumor detection with fluorescence intensity and lifetime imaging. *J Biomed Opt* **15**, 066012 (2010).
31. Goiffon, R.J., Akers, W.J., Berezin, M.Y., Lee, H. & Achilefu, S. Dynamic noninvasive monitoring of renal function in vivo by fluorescence lifetime imaging. *J Biomed Opt* **14**, 020501 (2009).
32. Hall, D.J.*, et al.* Dynamic optical imaging of metabolic and NADPH oxidase-derived superoxide in live mouse brain using fluorescence lifetime unmixing. *J. Cereb. Blood Flow Metab.* **32**, 23-32 (2012).
33. Wang, J.*, et al.* A novel brain metastases model developed in immunodeficient rats closely mimics the growth of metastatic brain tumours in patients. *Neuropathol. Appl. Neurobiol.* **37**, 189-205 (2011).
34. Taruttis, A. & Ntziachristos, V. Translational optical imaging. *AJR. American journal of roentgenology* **199**, 263-271 (2012).
35. Herron, T.J., Lee, P. & Jalife, J. Optical imaging of voltage and calcium in cardiac cells & tissues. *Circulation research* **110**, 609-623 (2012).